Comparison of Rainfall Products Derived from TRMM Microwave Imager and Precipitation Radar

HIROHIKO MASUNAGA*

Earth Observation Research Center, National Space Development Agency, Chuo-ku, Tokyo, Japan

TOSHIO IGUCHI

Applied Research and Standards Division, Communication Research Laboratory, Koganei, Tokyo, Japan

RIKO OKI

Satellite Program and Planning Department, National Space Development Agency, Minato-ku, Tokyo, Japan

MISAKO KACHI

Earth Observation Research Center, National Space Development Agency, Chuo-ku, Tokyo, Japan

(Manuscript received 2 November 2001, in final form 18 February 2002)

ABSTRACT

Satellite remote sensing is an indispensable means of measuring and monitoring precipitation on a global scale. The Tropical Rainfall Measuring Mission (TRMM) is continuing to make significant progress in helping the global features of precipitation to be understood, particularly with the help of a pair of spaceborne microwave sensors, the TRMM Microwave Imager (TMI) and precipitation radar (PR). The TRMM version-5 standard products, however, are known to have a systematic inconsistency in mean monthly rainfall. To clarify the origin of this inconsistency, the authors investigate the zonal mean precipitation and the regional trends in the hydrometeor profiles in terms of the precipitation water content (PWC) and the precipitation water path (PWP) derived from the TMI profiling algorithm (2A12) and the PR profile (2A25). An excess of PR over TMI in near-surface PWC is identified in the midlatitudes (especially in winter), whereas PWP exhibits a striking excess of TMI over PR around the tropical rainfall maximum. It is shown that these inconsistencies arise from TMI underestimating the near-surface PWC in midlatitude winter and PR underestimating PWP in the Tropics. This conclusion is supported by the contoured-frequency-by-altitude diagrams as a function of PWC. Correlations between rain rate and PWC/PWP indicate that the TMI profiling algorithm tends to provide a larger rain rate than the PR profile under a given PWC or PWP, which exaggerates the excess by TMI and cancels the excess by PR through the conversion from precipitation water to rain rate. As a consequence, the disagreement in the rainfall products between TMI and PR is a combined result of the intrinsic bias originating from the different physical principles between TMI and PR measurements and the purely algorithmic bias inherent in the conversion from precipitation water to rain rate.

1. Introduction

Satellite remote sensing is an efficient tool for measuring rainfall on a global scale. Techniques for evaluating precipitation from satellites may be divided into three major categories: those based on visible and/or infrared measurements, those based on passive-microwave measurements, and those based on radar measurements (Kidder and Vonder Haar 1995). The visible and/or infrared techniques rely on the assumption that a clear correspondence exists between the observed characteristics at cloud top and rain rates, whereas the microwave techniques directly detect precipitating hydrometeors in addition to the overlying cloud layer.

Rainfall measurements by spaceborne microwave radiometers have a long history (e.g., Wilheit et al. 1977, 1991; Spencer 1986; Olson 1989; Kummerow and Giglio 1994; Aonashi et al. 1996; Kummerow et al. 1996). Current widely used sensors for satellite microwave radiometry of precipitation are the Special Sensor Microwave Imager (SSM/I) aboard the Defense Meteorological Satellite Program satellites and the Tropical Rainfall Measuring Mission (TRMM) Microwave Imager (TMI) aboard the TRMM satellite. In addition to TMI, the TRMM satellite has the advantage of carrying the pre-

* Current affiliation: Department of Atmospheric Science, Colorado State University, Fort Collins, Colorado.

Corresponding author address: Hirohiko Masunaga, Department of Atmospheric Science, Colorado State University, Fort Collins, CO 80523.
E-mail: masunaga@atmos.colostate.edu

© 2002 American Meteorological Society

cipitation radar (PR), which is a unique spaceborne radar used to measure rainfall and is capable of profiling precipitation with a vertical resolution of 250 m. TMI and PR can independently estimate precipitation. The two estimations ideally should agree with each other.

The TRMM standard products provided by the National Aeronautics and Space Administration (NASA) Goddard Space Flight Center (GSFC) support rain rates near the surface (hereinafter called simply rain rates) evaluated either from TMI or PR or from their combined use (Kummerow et al. 2000). Kummerow et al. (2000) investigated consistency among the TRMM standard products for precipitation and found a bias of 24% in the global tropical monthly averages of rain rate in the latest version (version 5) of the products. The largest discrepancy lies between the products derived from the TMI profiling algorithm (2A12) and the PR profile (2A25), where the former provides the maximum rain rates in the Tropics and the latter the minimum. The discrepancies in the rainfall products are among the major problems to be resolved to achieve the scientific goals of TRMM, such as evaluating the latent heat over the global Tropics (Tao et al. 2001).

There are a number of possible sources of the disagreement in estimated rain rates. First, the disagreement may be attributed to the difference between a radiometer and a radar in the physical principles for sensing rainfall. A radar directly measures the three-dimensional structure of precipitation. In contrast, some model assumptions in the retrieval algorithm are required to derive the vertical structure from brightness temperatures detected by a radiometer. Radar measurements basically involve only the backscattering and attenuation of microwaves. Radiometric measurements, however, are more complicated because brightness temperatures can be enhanced by the thermal emissions, can be shielded by the scattering, or there may be a trade-off between them, depending on the channel frequency and the phase of hydrometeors (liquid, ice, or their mixture). TMI has nine channels at five frequencies from 10.65 to 85.5 GHz, with vertical and horizontal polarizations for each, except for the 21.3-GHz channel. Precipitation radar, in contrast, is a single-frequency (13.8 GHz) radar. As a result, PR is insensitive to ice particles unless they are large enough to be detectable by 2.2-cm wavelength microwaves. Difference in the footprint size between the sensors also could produce a disagreement in the retrievals. TMI retrievals may suffer from the nonuniform beam-filling effect more seriously than PR does because of the large footprint sizes for the low-frequency channels of TMI (e.g., 63 km in the down-track direction at 10.65 GHz) as compared with the PR footprint size (4.3 km for nadir).

Second, one may focus on uncertainties that depend on model assumptions involved with individual retrieval algorithms. A possible source of the uncertainties arises from the treatment of drop size distributions (DSDs; Viltard et al. 2000). The TMI profiling algorithm (2A12) is based on the Bayesian approach to derive hydrometeor profiles by comparing the observed brightness temperatures with a preexisting database (Kummerow et al. 1996; Olson et al. 1996). In treating DSDs, the 2A12 algorithm relies on assumptions in the cloud-resolving models used to construct the database. Uncertainties in the DSD assumptions are not critical in TMI measurements because TMI brightness temperatures in low-frequency channels are insensitive to DSD, but DSD will become important later when the conversion from precipitation water to rain rate is discussed. In contrast, the PR 2A25 algorithm employs a globally averaged DSD as the initial guess to obtain the radar reflectivity–rain rate (Z–R) and specific attenuation–radar reflectivity (k–Z) relations adjusted to be consistent with the assumed DSD model (Iguchi et al. 2000). The DSD assumptions more strongly affect PR retrievals than those from TMI because information on the DSD enters radar echoes through the sixth moment of the DSD instead of the third moment. Viltard et al. (2000) investigated the consistency in observed and synthesized brightness temperatures using TRMM data, where the synthesized brightness temperatures were simulated in the use of the PR profiles, to examine the sensitivity to the assumptions on DSDs. In addition to the ambiguities in treating DSDs, other types of algorithm-dependent error sources include limitation in the universality of model databases and ambiguity in the attenuation correction. These algorithmic problems, in particular the DSD uncertainties, and the differences in measurement principle and footprint size are crucial. They are outside the scope of this paper but should be investigated in future studies.

In addition to the algorithmic differences, one must consider the definition of rain rate itself as a candidate source of the uncertainty. The rain rate is theoretically proportional to

$$\int_0^\infty v(D)n(D)D^3\,dD, \tag{1}$$

where $v(D)$ is the fall velocity of a raindrop with diameter D, and $n(D)$ is the DSD. Because neither TMI nor PR can measure the fall velocity directly, accuracy in estimating rain rate is limited by the uncertainties in $v(D)$. This point has important implications. In particular, the TMI brightness temperatures do not strongly depend upon the details of the DSD, surface rainfall, on the other hand, does. We therefore prefer directly measurable quantities, such as the precipitation water content, for comparison between TMI and PR. Correlation between precipitation water content and rain rate is investigated below for each of the TMI and PR products.

In section 2, we describe the data employed in our analysis. Results are shown and some related discussions are presented in section 3, where results are compared in terms of the zonal-mean precipitation water

TABLE 1. Coefficients for the Z–W relation in (2) used in our calculations for the water content W (g m^{-3}) and the radar reflectivity Z (dBZ). The five node points A–E represent typical positions in precipitation profiles and are defined based on the phase and temperature of hydrometeors and on the rainfall types (stratiform, convective, and others). See Iguchi et al. (2000) for a detailed description of the node points.

	Stratiform		Convective		Others	
Nodes	a_w	b_w	a_w	b_w	a_w	b_w
A	0.003 836 13	0.712 66	0.006 208 68	0.689 02	0.006 208 68	0.689 02
B	0.003 250 46	0.704 72	0.003 917 52	0.578 55	0.005 371 14	0.680 04
C	0.000 743 01	0.665 64	0.003 917 52	0.578 55	0.003 917 52	0.578 55
D	0.001 998 06	0.613 42	0.003 917 52	0.578 55	0.003 917 52	0.578 55
E	0.002 237 87	0.596 58	0.004 444 52	0.562 32	0.004 444 52	0.562 32

contents and precipitation water paths (section 3a) and of the contoured-frequency-by-altitude diagrams (section 3b), followed by a brief examination of their correlation with rain rates (section 3c). The findings are summarized in section 4.

2. Data

As mentioned in section 1, the 2A12 and 2A25 rain rates have the largest disagreement among all the TRMM standard rainfall products (Kummerow et al. 2000). We therefore compare 2A12 and 2A25 in this study. In the 2A12 algorithm, the hydrometeor profiles are retrieved by relating the observed brightness temperatures to a large number of profiles in a preexisting database through the Bayesian inversion scheme (Kummerow et al. 1996; Olson et al. 1996). The database is computed from cloud-resolving models, such as the Goddard Cumulus Ensemble Model, that have been tested well for tropical convective systems (Kummerow et al. 1996). The 2A12 data contain the hydrometeor profiles for precipitation water, precipitation ice, cloud liquid water, and cloud ice water, all of which are in units of grams per cubic meter, and the latent-heat profile. The profiled quantities are assigned in 14 layers from the surface to 18 km in altitude. The near-surface rain rate is also included in the 2A12 products. In this paper, we mainly use the precipitation water and the precipitation ice to study consistency with the PR products and subsequently investigate the correlation of the water contents with the near-surface rain rate.

For comparison with the TMI products, we also need to derive the precipitation water and ice from the PR reflectivity, but the 2A25 dataset includes only the rain-rate profiles evaluated through the Z–R relations, not the water/ice contents. We therefore derived the Z–W relations to connect Z with the water content W, based on the DSD model consistent with the 2A25 algorithm in version 5 (Iguchi et al. 2000). [We note that the attenuation-corrected reflectivity, or Z_e using the notation in Iguchi et al. (2000), is denoted by the radar reflectivity Z in this paper.] The Z–W relations, like the Z–R relation, are expressed in a power-law relation,

$$W = a_w Z^{b_w}. \quad (2)$$

Coefficients a_w and b_w depend on the water temperature for rain and on the fractional abundance of water for a snow–water mixture. They are listed in Table 1 for each of convective, stratiform, and other rains, according to the specification for the 2A25 rain-rate profile [see Fig. 4 in Iguchi et al. (2000)].

We chose only the central 21 rays from the 49 rays within a PR swath because the near-surface quantities retrieved by PR are liable to be degraded in quality for large viewing angles near both ends of a scan line. We correspondingly omitted TMI footprints that do not overlap the selected PR beams (i.e., the central 21 rays) from the analysis to reduce errors due to the difference in the sampling swath between TMI and PR.

The 2A12 and 2A25 datasets are then assigned to a common format of the spatial allocation. The 2A25 data profiles with 250-m resolution are readjusted, by averaging, to the 14 layers that correspond with the 2A12 profiling format. The 2A12 and 2A25 data at the satellite footprint level are gridded to 0.5-°^{2} resolution by the spatial average inside every grid box. Monthly mean data are obtained after the above-mentioned data processing is performed for every satellite orbit. In this paper, we present two sets of monthly data (July of 1998 and January of 1999). Neither of these months is affected by the El Niño event that occurred from 1997 to early 1998 because the event had ceased by July of 1998. The data are therefore considered to represent the climatological trend, although they may be somewhat influenced by the La Niña event that followed the El Niño in 1998.

Although it would be interesting to discuss, we do not include the 2B31 product (i.e., the combined TMI/PR rainfall) in this study. This is because of the technical reason that the 2B31 product is not designed to allow us to estimate the precipitation-water profiles instead of the rain-rate profiles.

3. Results and discussion

In this section, we present and compare the rainfall retrievals derived by the TMI (2A12) and PR (2A25) algorithms. Hereinafter, TMI and PR refer to products/algorithms specifically of 2A12 and 2A25, respectively,

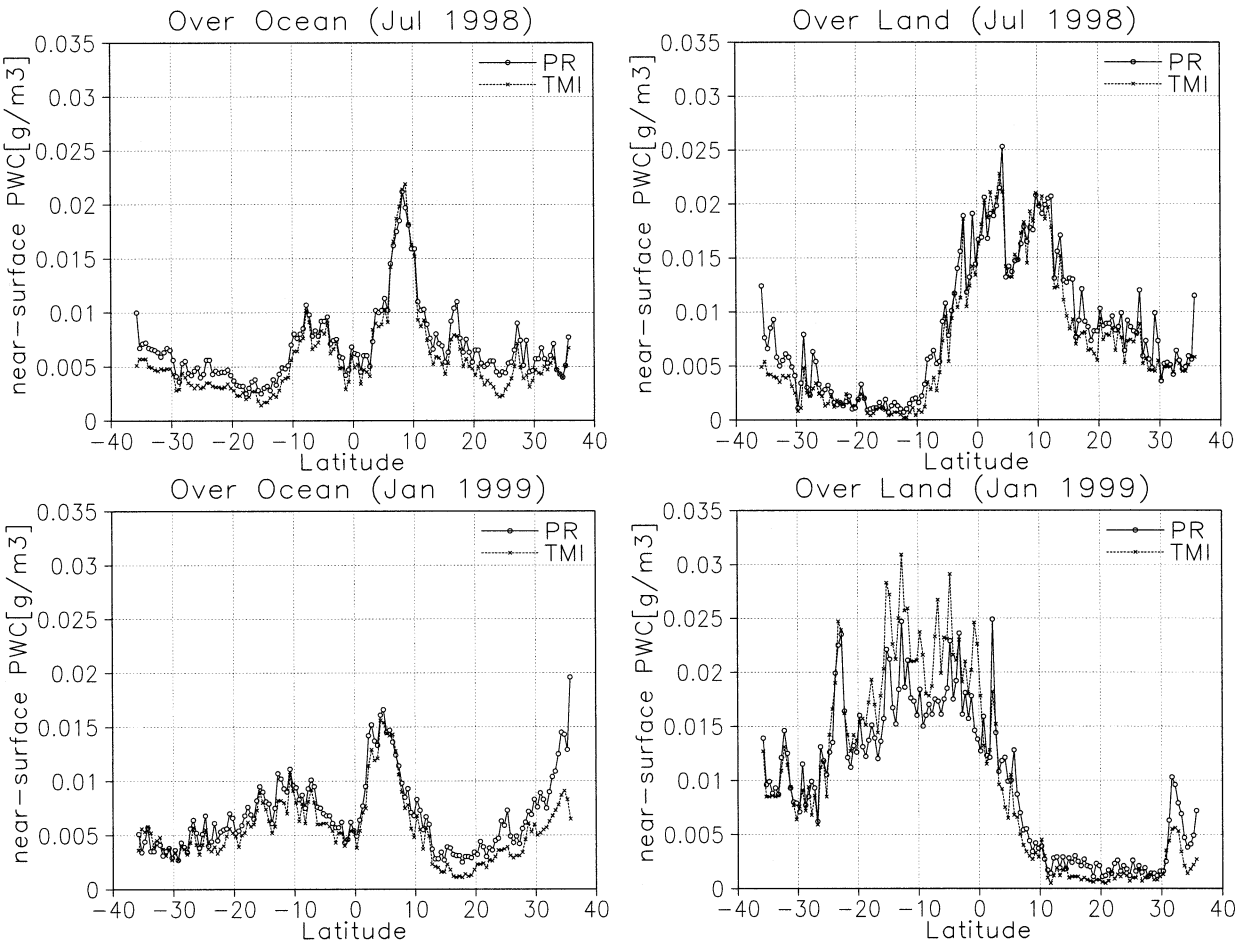

FIG. 1. The zonal mean PWC near the surface (in the 0–500-m layer) over (left) ocean and (right) land in (top) Jul 1998 and (bottom) Jan 1999.

unless otherwise noted. The TMI and PR products are compared in terms of the precipitation water instead of the rain rate, which is usually of interest, as noted in section 1. In section 3a, the precipitation water content (PWC), or the mass density of precipitation water per unit volume, and the precipitation water path (PWP), defined as

$$\mathrm{PWP} = \int_0^h \mathrm{PWC}(z)\, dz,$$

where z is the altitude and $h = 18$ km is the top altitude of the highest 2A12 layer, are presented in the zonal mean. The precipitation water content near the surface in the 0–500-m layer is called simply PWC_{ns}. In section 3b, differences in the statistical trend of the rainfall profiles between the TMI and PR products are investigated. Correlation between PWC_{ns}/PWP and rain rate is examined in section 3c.

a. Zonal mean precipitation water

The zonal mean PWC_{ns} and PWP estimated from TMI and PR are shown in Figs. 1 and 2, where the TMI retrievals include only the liquid-water component. We have excluded the precipitation ice to achieve a straightforward comparison with the PR-derived quantities because an appreciable fraction of ice particles is undetectable by PR. Effects of including the precipitation ice in the TMI products will be demonstrated for reference in the last part of this section (Fig. 3) and in section 3b.

Figure 1 shows excellent agreement in PWC_{ns} between TMI and PR over tropical oceans. A systematic excess of PR-derived PWC_{ns} (PR-PWC_{ns}) over TMI-derived PWC_{ns} (TMI-PWC_{ns}) is observed in the midlatitudes, and more clearly so in the winter hemisphere. This tendency is most conspicuous at latitudes above 30°N in January. Although the data are somewhat noisy, PWC_{ns} over land is similar to that over oceans except

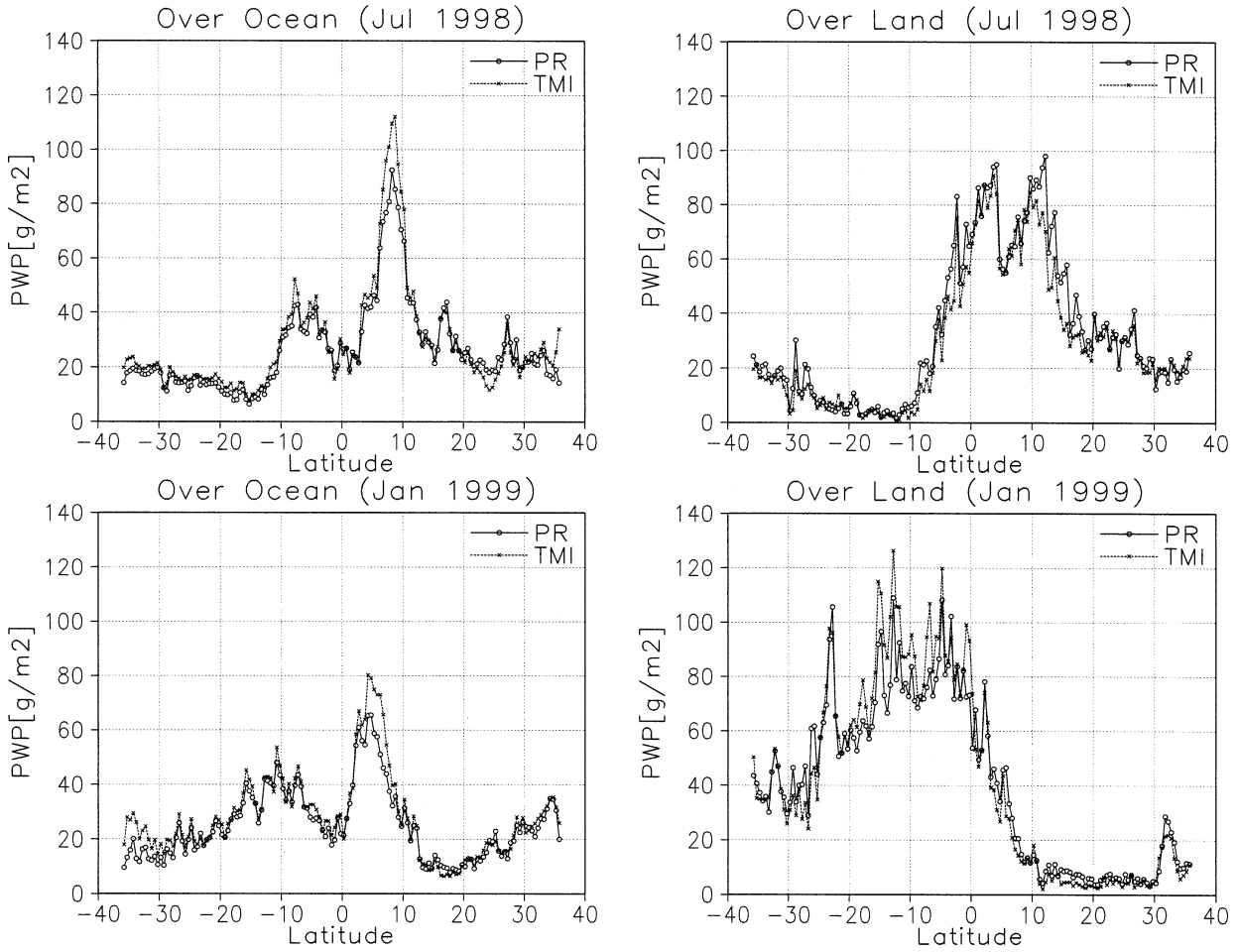

FIG. 2. Same as Fig. 1, but for the zonal mean PWP.

for the region of 20°S to 0° in January, in which TMI-PWC_{ns} is larger than PR-PWC_{ns}. It is noted that the land rainfall is in remarkable agreement despite the limitation of radiometer measurements of continental rainfall. This result may be because the TMI land algorithm employs the database constituted of the rainfall profiles that were carefully selected in comparison with ground measurements (see also section 3b).

Figure 2 illustrates the difference between PWPs derived from TMI and PR (TMI-PWP and PR-PWP), showing a remarkable contrast to Fig. 1. TMI-PWP and PR-PWP agree very well in the oceanic environment except for the region with the maximum PWP in the Tropics (0° to 10°N), in which TMI-PWP exceeds PR-PWP by about 20%. Characteristic patterns of PWP over land resemble those of PWC_{ns} for TMI and PR, although the excess of PR in PWC_{ns} seen in the midlatitudes has been reduced in PWP.

In summary, there are two notable differences in the precipitation water between the TMI and PR products: 1) PR exceeds TMI in PWC_{ns} in midlatitude winter and 2) TMI exceeds PR in PWP around the tropical rainfall maximum. In either case, the discrepancy is presumed to be caused by inconsistencies in the hydrometeor profiles derived by the TMI and PR algorithms. Although there is no way to determine whether TMI or PR retrieves PWC_{ns} and PWP more accurately, we address a hypothetical solution from the viewpoint of the physical principles in radiometric and radar remote sensing.

- PR should be more reliable in retrieving PWC_{ns} than TMI is because PR echoes more directly evaluate the hydrometeor profiles than do TMI brightness temperatures.
- TMI brightness temperature at 10 GHz is preferable to PR echoes for estimating PWP because the thermal emissions are less sensitive to the DSD assumptions and are less damaged by a heavy extinction than is the scattered radiation. On the other hand, the correlation between PWP and the 10-GHz brightness temperature would suffer from the poor spatial resolution of the 10-GHz channel. Nevertheless, the TMI algorithm overcomes this difficulty to some extent with the help of the high-frequency channels.

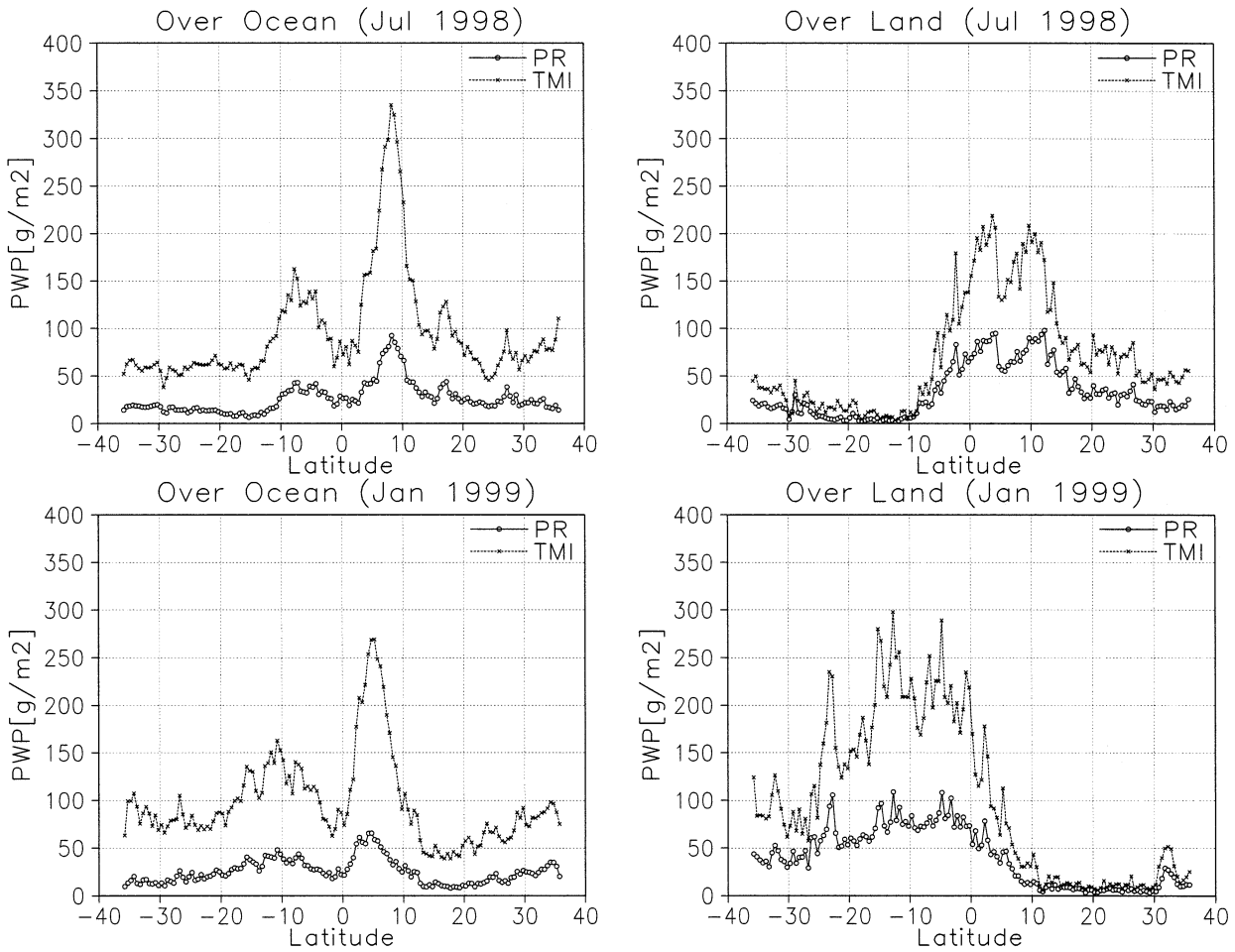

FIG. 3. Same as Fig. 2, but including the precipitation ice for TMI-PWP.

In this context, TMI would underestimate the midlatitude rainfall and PR would underestimate the tropical maximum of precipitation. In the next section, we examine characteristic differences in the rainfall profiles between TMI and PR to validate this hypothesis.

Before closing this section, we demonstrate for reference how much precipitation ice PR misses as compared with TMI in Fig. 3. There is a large difference in the sensitivity to ice particles between TMI and PR. Sensitivity of PR to hydrometeors depends on the particle-size effect (the backscattering cross section $\propto D^6$ in the Rayleigh regime) and on the dielectric property of scattering particles. For the dielectric property, liquid water is about 4 times as large as ice in the Rayleigh backscattering cross section, which accounts for the insensitivity of PR to ice particles in combination with the particle-size effect. Whereas ice particles are detectable by PR if they are sufficiently large, TMI is sensitive to smaller ice hydrometeors as well by virtue of the high-frequency channels. This difference in the detectability of ice between TMI and PR results in a large discrepancy in the estimated ice amount.

Figure 3 is the same as Fig. 2, but the precipitation ice is included in the TMI retrieval. Addition of the ice component leads to a drastic increase in global TMI-PWP except for the subtropics over lands in the dry season. Adding precipitation ice does not cause any apparent change in TMI-PWC_{ns} (not shown), because the contribution of snow is negligible near the surface throughout the latitude range observable from the TRMM satellite.

b. Vertical profiles of precipitation water

The results obtained in the previous section motivate us to examine characteristics in the vertical profiles of hydrometeors retrieved by TMI and PR. In this section, we investigate statistical trends in the vertical profiles of PWC using contoured-frequency-by-altitude diagrams (CFADs). The abscissa conventionally represents the radar reflectivity in a CFAD, but radar reflectivity is replaced by PWC in this work.

Figures 4–7 present CFADs for some representative sites listed in Table 2. Each figure consists of three

TABLE 2. Area coverages for the four representative sites adopted in section 3b.

Sites	Area definitions
Western Pacific	5°–20°N, 130°–165°E over ocean
Eastern Pacific	15°S–15°N, 130°–90°W over ocean
South America	35°S–10°N, 80°–45°W over land
Midlatitude Pacific	20°–35°N, 120°–165°E over ocean

panels showing PR-PWC (left), TMI-PWC without ice (middle), and TMI-PWC including the precipitation ice (right). All data are based on monthly statistics in January of 1999.

Figure 4 represents a heavily precipitating region close to the western Pacific warm pool. In the TMI-PWC profiles, the freezing level is clearly identified at an altitude of about 4 km, above which PWC in the liquid phase decreases rapidly with increasing height and disappears completely at 9 km in altitude (Fig. 4, middle), as an appreciable amount of the precipitation ice takes its place up to (or beyond) the tropopause (Fig. 4, right). The PR-PWC profiles, in contrast, show that PWC gradually and monotonically decreases with increasing height without discontinuity at the freezing layer as identified by TMI (Fig. 4, left). A straightforward comparison between the TMI- and PR-derived profiles is therefore not easy because of the difference in the detectability of pure ice particles between TMI and PR as mentioned at the end of the previous section, and the PR-derived profile is expected to correspond to an intermediate profile between extremes as shown by the middle and right panels in Fig. 4. However, comparison is meaningful for the domain where hydrometeors are all melted, or below a typical freezing level of 4–5 km in the Tropics. PR echoes detected far above the freezing levels are attributed to a small but finite fraction of very large frozen hydrometeors.

Figure 5 presents a CFAD for an eastern Pacific region containing the ITCZ. As expected, both the left and right panels indicate that average heights of rainfall tend to be relatively lower than in the western Pacific (Fig. 4), whereas the freezing level appears to show no substantial difference between the western and eastern Pacific regions (middle panel).

In Figs. 4 and 5, PWC tends to be systematically larger 3–4 km above the surface for TMI than for PR while the frequency distributions of PWC are similar near the surface. This behavior explains the tropical characteristics in the zonal mean precipitation water, that is, the excellent agreement in PWC_{ns} and the large excess of TMI-PWP over PR-PWP around the tropical rainfall maximum (cf. section 3a).

PWC profiles over the South American continent are illustrated in Fig. 6. The PR and TMI (with ice) profiles consistently indicate that precipitation is often developed at higher altitudes than oceanic rainfall is (Figs. 4 and 5), as expected for continental precipitation. The liquid precipitation water cuts off more sharply above 4 km in the TMI profiles than in the tropical oceanic cases. It is reasonable that the continental rainfall profiles are still more homogeneous than the oceanic rainfalls in the TMI products because the TMI land algorithm employs a limited number of profiles in the database that were carefully selected so that the satellite-retrieved rain rate by the scattering scheme (i.e., using

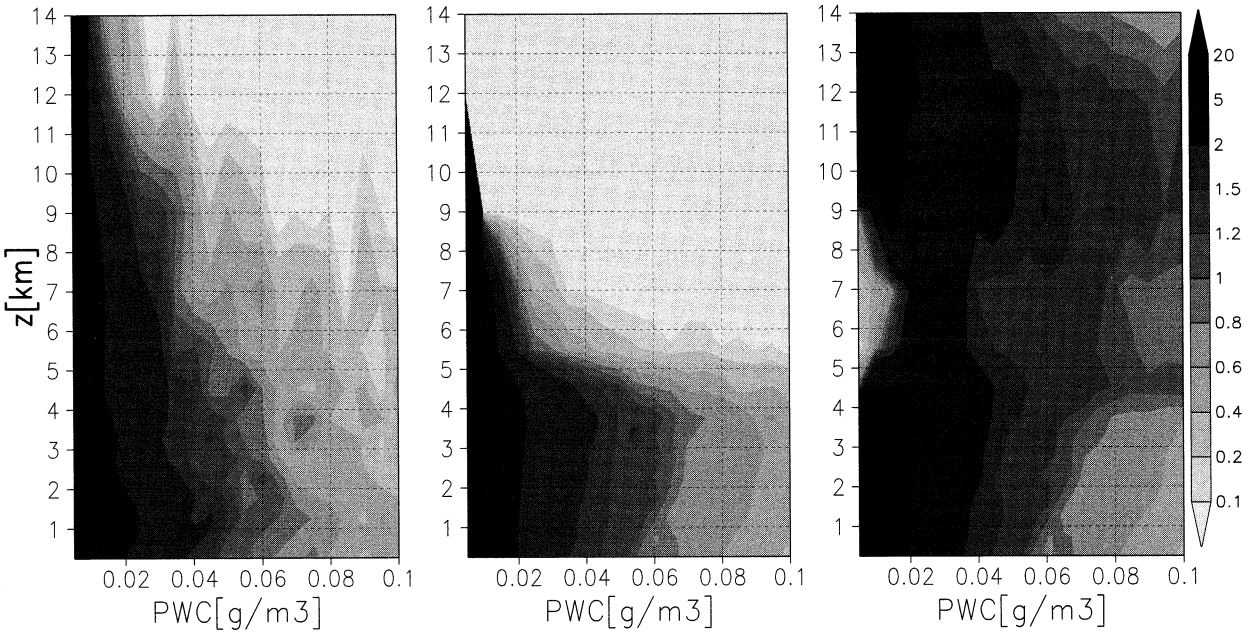

FIG. 4. CFAD for PWC, as abscissa, at the western Pacific site (cf. Table 2) in Jan 1999: (left) PR-PWC profile, (middle) TMI-PWC profile without ice, and (right) TMI-PWC profile including the precipitation ice.

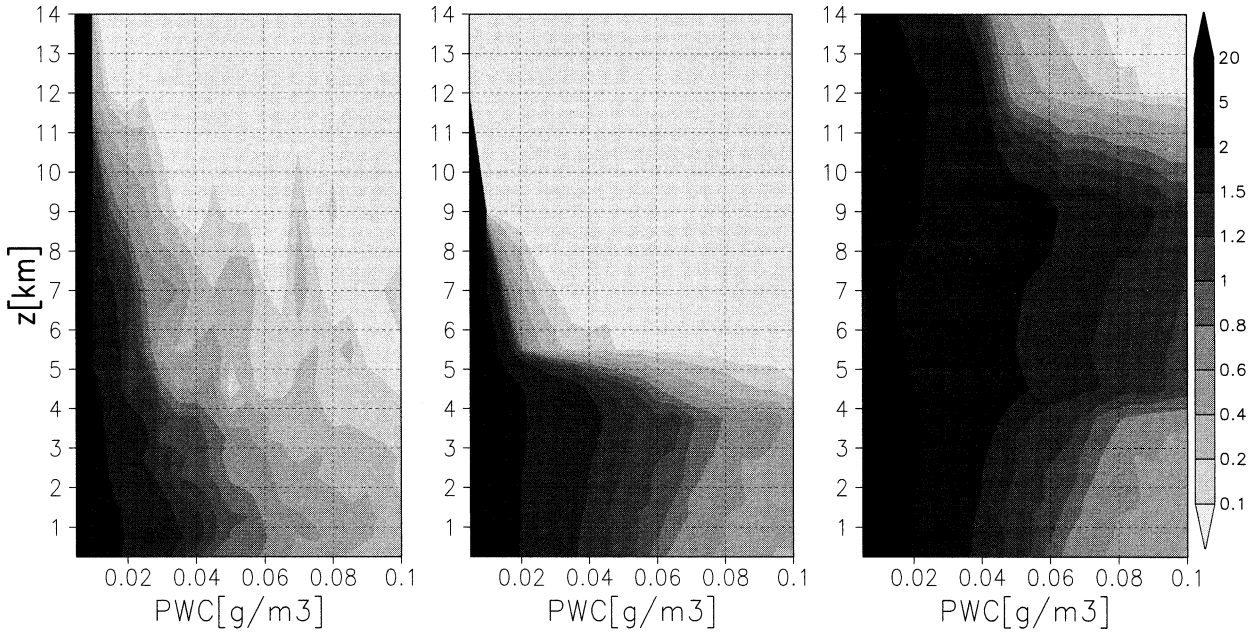

FIG. 5. Same as Fig. 4, but at the eastern Pacific site (cf. Table 2).

the 85-GHz brightness temperature) should be consistent with ground-radar measurements.

Figure 7 illustrates the northern midlatitude Pacific precipitation. The PWC profile acquired by PR exhibits very different characteristics from those shown above (Figs. 4–6). This is reasonable in the context of the variance in the precipitation mechanisms between tropical convection systems and midlatitude storms. A peak at 1 km above the surface in the CFAD by PR is presumed to result from significantly lower heights of rainfall than in the tropical Pacific and South American cases. In contrast, TMI shows much less variety in the PWC profiles, except for the double peaks in the precipitation ice profile at 2–4 and 12 km in height seen in Fig. 7. The freezing level at 1 km in height cannot be reproduced by the TMI algorithm because the TMI

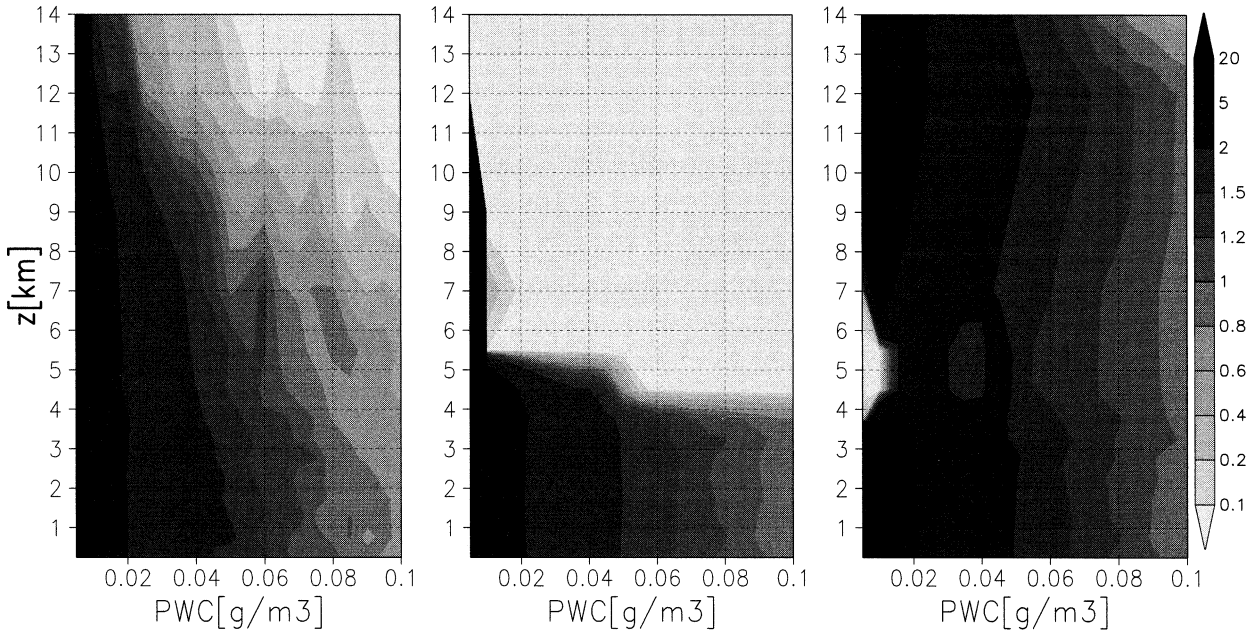

FIG. 6. Same as Fig. 4, but at the South American site (cf. Table 2).

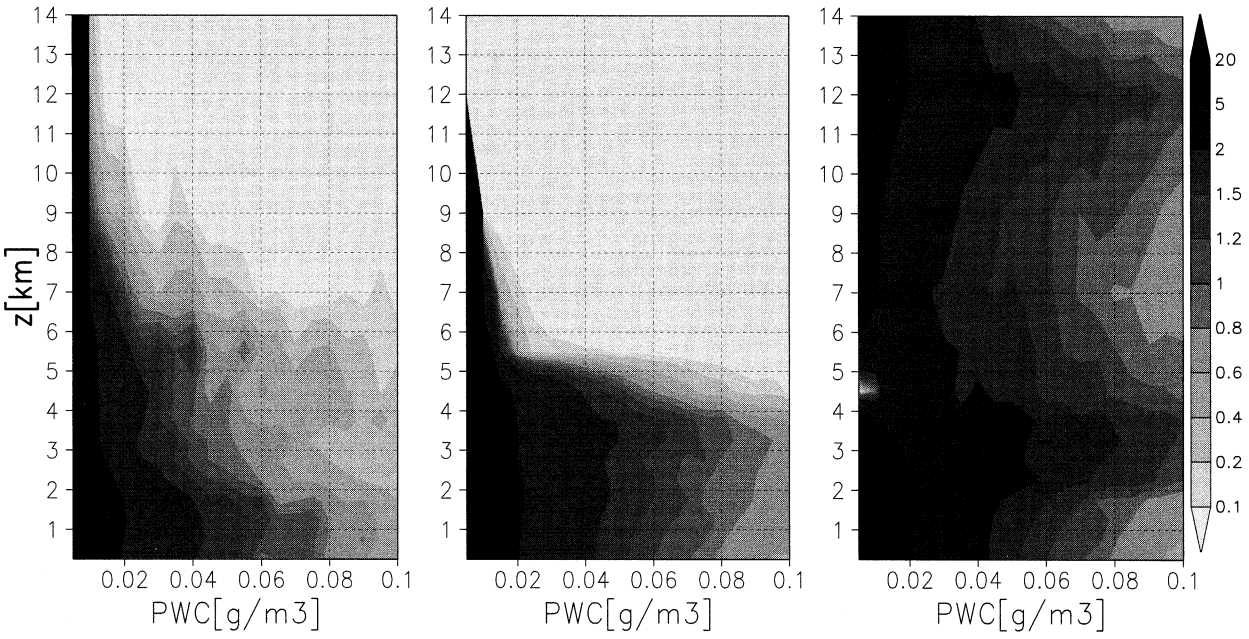

FIG. 7. Same as Fig. 4, but at the midlatitude Pacific site (cf. Table 2).

algorithm outside the Tropics is represented by a discrete set of raining profiles that have freezing levels at 3.5, 2.9, and 2.3 km, which probably account for the lower TMI peak (2–4 km). The other TMI peak, at a height of 12 km, seems unrealistic for precipitation in midlatitude winter, and reminds us of tropical convective precipitation rather than a midlatitude storm. In the middle panel of Fig. 7, the freezing level is frequently identified at a height of 4 km, which also reminds us of tropical rainfall.

We now revisit the hypothesis addressed in section 3a. It implies that the tropical rainfall maximum should be estimated more accurately by TMI and underestimated by PR and that the midlatitude rainfall should be derived more precisely by PR and underestimated by TMI. This hypothesis is consistent with the fact that the preexisting database in the TMI profiling algorithm (2A12) is based on the cloud-resolving models focusing mainly on the tropical rainfall system (Kummerow et al. 1996). The PWC profiles by TMI are acceptable for tropical precipitation (Figs. 4 and 5). Examination of Fig. 7 reveals that PWC is reasonably concentrated near the surface in the PR-derived profile but that TMI redistributes the precipitation water into a more vertically homogeneous profile, although the vertically integrated PWC (or PWP) agrees well in this region according to Fig. 2. The discrepancy in PWC is inferred to result from failure in the profiling by TMI. This may be because the model database in the TMI algorithm does not completely cover the actual variation in precipitation profiles, particularly for precipitation types differing from those typical in the Tropics.

Furthermore, the hypothesis above does not contradict the tendency that PR measurements are subject to uncertainties in the attenuation correction, especially for the heavy precipitation typical in the Tropics, which could increase errors in estimating PWC and PWP by PR. If the radar reflectivity is damaged by a heavy extinction, it would lead to a notable disagreement in the retrieved rainfall between TMI and PR in the Tropics as observed in PWP (Fig. 2). In contrast, PWC_{ns} shows an excellent agreement in the Tropics (Fig. 2). In fact, the near-surface quantities would be less seriously degraded in accuracy than the off-surface quantities by virtue of the surface reference technique used for the attenuation correction. In the surface reference technique, the path-integrated attenuation (PIA) is estimated by comparing the surface echoes in the precipitating area with those in a rain-free area (Meneghini et al. 2000). Under a given constraint on PIA, PWC_{ns} is evaluated more precisely than off-surface PWCs, for which the attenuation correction would be less accurate because of the uncertainty in the vertical extinction profile. The PR algorithm (2A25) depends on the surface reference technique to avoid numerical difficulties encountered when solving the Hitschfeld–Bordan equation for the attenuation correction in heavy-precipitation regions (Iguchi et al. 2000).

As a result, it is plausible that the TMI algorithm tends to underestimate PWC in the midlatitudes (especially in the winter hemisphere) and that the PR algorithm tends to underestimate PWP in the tropical rainfall maximum, as predicted by the hypothesis raised in section 3a. Our next step is to investigate how the rain rate relates with PWC and PWP, which is the subject of the subsequent section.

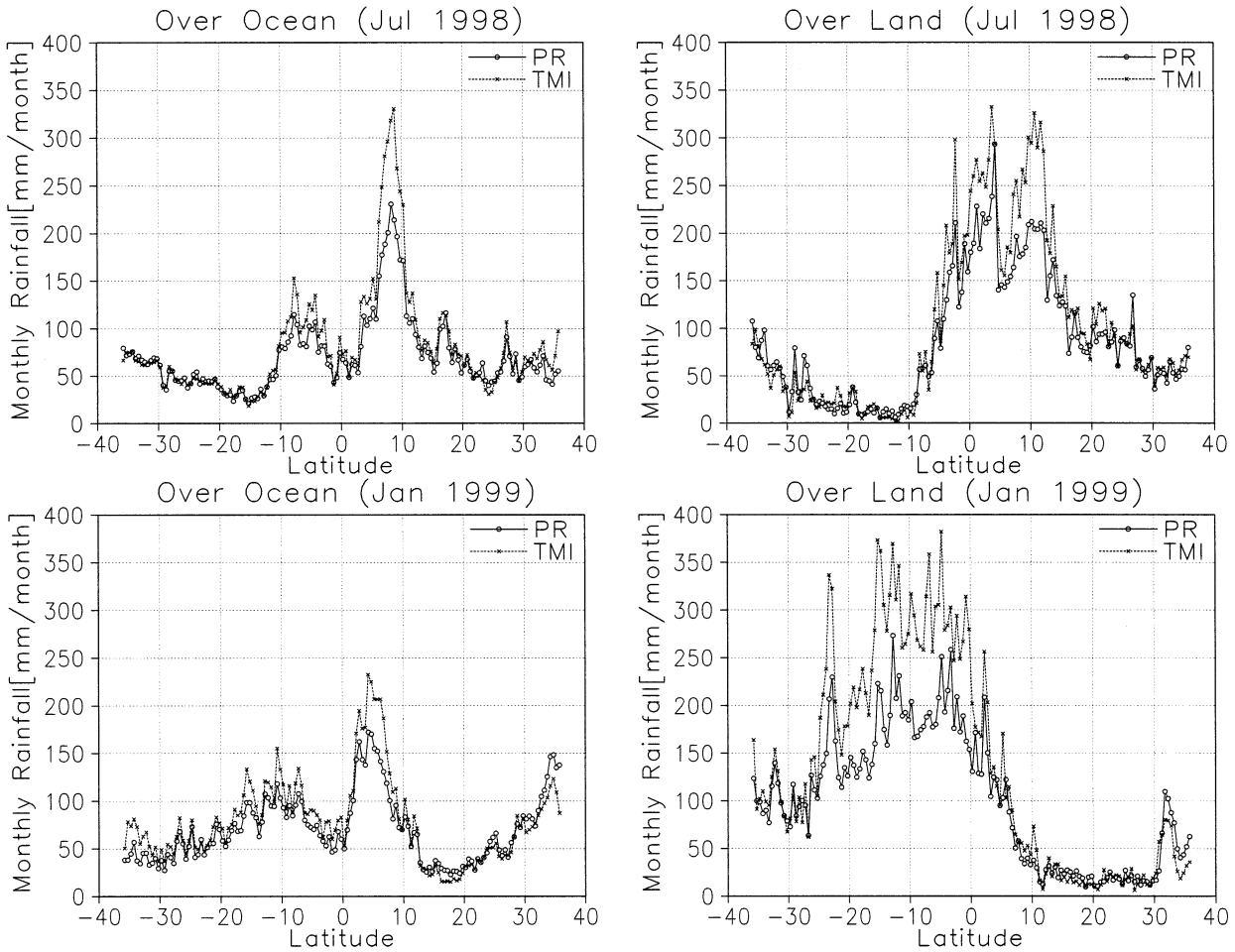

FIG. 8. Same as Fig. 1, but for the zonal mean rain rate near the surface.

c. Correlation between rain rate and precipitation water

A major concern of meteorologists and hydrologists engaged in precipitation studies is the rain rate rather than PWC and PWP. In this section, we examine the correlation between rain rate and precipitation water to discuss the influences of the results obtained in the preceding sections.

Figure 8 shows the zonal mean monthly rain rates derived from the TMI and PR products. One can immediately find a considerable excess of the TMI rain rate over the PR rain rate around the tropical maximum, which obviously reflects the tendency in PWP (Fig. 2). A small excess of PR is identified in the northern midlatitude in January of 1999 in accordance with the trend in PWC_{ns} (Fig. 1), although the discrepancy is less pronounced in rain rate than in PWC_{ns}. This excess of PR disappears, or is inverted, in July, and hence the discrepancy in the midlatitude rain rates is almost canceled in the annual average. The overall features in Fig. 8 are consistent with Kummerow et al. (2000), who found that the disagreement in the tropical-mean monthly rain rates over oceans in 1998 is 24% among the TRMM standard algorithms in version 5 (Fig. 4 of Kummerow et al. 2000). As compared with Fig. 8, the region with a large difference in rain rate extends over a broad region over tropical oceans in Kummerow et al. (2000), which is deemed to be affected by the anomaly in tropical precipitation due to the El Niño event.

The excess of TMI in rain rate over PR around the tropical rainfall maximum seems to be reasonably interpreted to result from a similar feature in PWP (Fig. 2). However, it is still curious why PWC_{ns}, which should be more closely related with near-surface rain rate than PWP, shows no sign for such excess in the Tropics (Fig. 1). This result implies the presence of an algorithmic bias in the conversion from precipitation water to rain rate in addition to the intrinsic bias inherent in PWP and PWC_{ns}.

Some differences in the assumptions underlying both the algorithms could produce a bias in the conversion

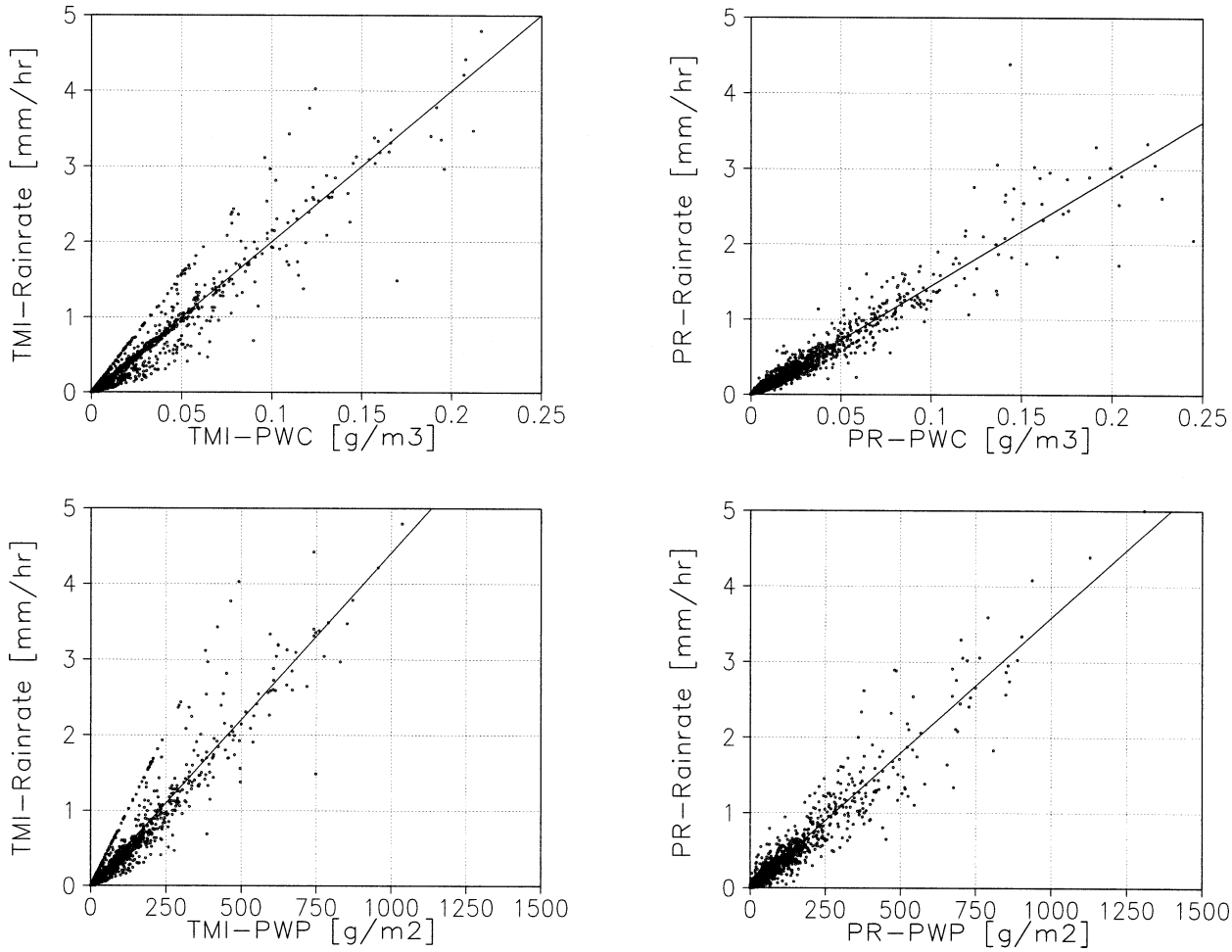

FIG. 9. Scatter diagrams for (top) rain rate vs PWC_{ns} and (bottom) rain rate vs PWP for the (left) TMI profiling algorithm and (right) PR profile.

from precipitation water to rain rate. First, the TMI and PR algorithms are based on different DSD assumptions. The PR algorithm assumes a gamma distribution for the DSD model to derive the *Z–R* relations for each rain type (i.e., stratiform, convective, and others). In contrast, the TMI algorithm adopts the Marshall–Palmer distribution for the DSD. Second, the definitions of precipitation water and rain rate are based on different physical backgrounds between TMI and PR. The retrievals are ''physical'' outputs given by model simulations in the TMI rainfall products, whereas rainfall quantities are directly connected with the radar reflectivity through the *Z–R* and *Z–W* relations in the PR algorithm.

Figure 9 demonstrates the correlation between the rain rate and the precipitation water over the globe for the TMI (without ice) and PR products. The best-fit linear functions for the scatter plots, delineated in Fig. 9, are found to be

$$\mathrm{RR} = \begin{cases} -0.0053 + 20.0\mathrm{PWC}_{ns} & \text{for TMI} \\ -0.0033 + 14.5\mathrm{PWC}_{ns} & \text{for PR} \end{cases} \quad \text{and} \tag{3}$$

for PWC_{ns} (g m^{-3}) and

$$\mathrm{RR} = \begin{cases} -0.0084 + 0.004\,42\mathrm{PWP} & \text{for TMI} \\ 0.0001 + 0.003\,58\mathrm{PWP} & \text{for PR} \end{cases} \quad \text{and} \tag{4}$$

for PWP (g m^{-2}), where RR is the rain rate (mm h^{-1}).

In both (3) and (4), TMI tends to have a larger inclination of the best-fit line than PR does, and the offset is negligibly small in every case. In other words, TMI tends to yield a higher rain rate than PR in response to a given PWC_{ns} or PWP, and the difference increases as the precipitation becomes heavier, as demonstrated by taking the difference between TMI and PR in (3) and (4):

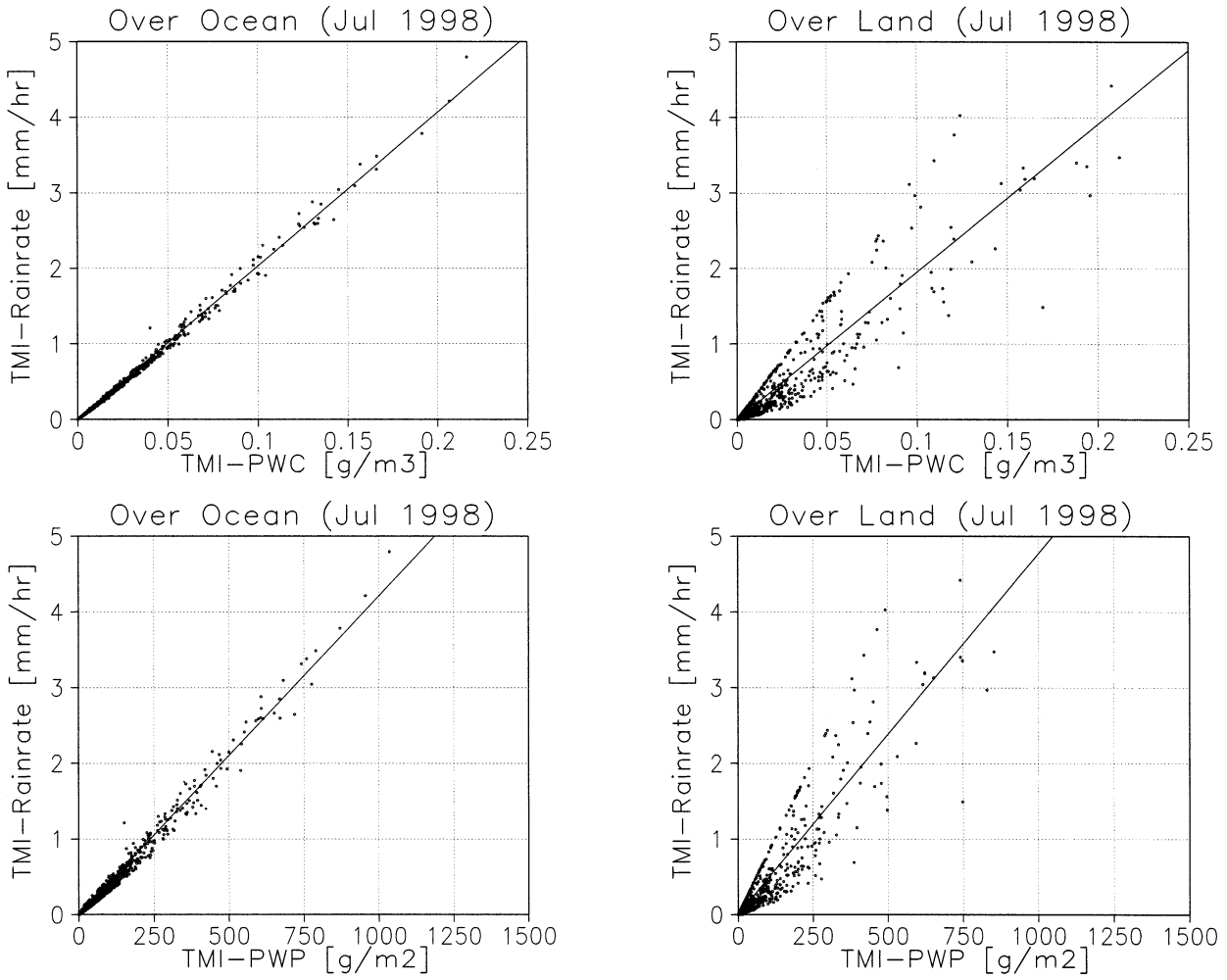

FIG. 10. Similar to Fig. 9, but each shown separately for (left) oceanic and (right) continental rainfalls for the TMI profiling algorithm.

$$\Delta RR(TMI - PR) = \begin{cases} -0.0020 + 5.5PWC_{ns} & \text{for } PWC_{ns} \text{ and} \\ -0.0085 + 0.000\,84PWP & \text{for PWP.} \end{cases} \quad (5)$$

As a consequence, the excess of TMI over PR in precipitation water would be expanded in rain rate and vice versa, although these trends would not be notable in low-precipitation regions. This accounts for the trend found in Fig. 8, where the excess of TMI over PR around the tropical rainfall maximum, which originated from the feature appearing in PWP (Fig. 2), is exaggerated in rain rate while the midlatitude excess of PR over TMI in PWC_{ns} is suppressed in rain rate. We thus conclude that the large excess of TMI over PR in tropical rainfall results from a combined effect of the intrinsic retrieval bias in PWP and an algorithmic bias in the conversion from PWP to rain rate. Excess of PR in midlatitude PWC_{ns}, in contrast, appears to be compensated by an opposite bias in the rain rate–PWC_{ns} relation. The coincidence in rain rate between TMI and PR in the midlatitudes thus seems to be a fortunate artifact rather than a successful agreement between the algorithms.

One might wonder if the correlation between rain rate and precipitation water depends on the surface condition (i.e., ocean or land) for TMI measurements because of the difference in algorithmic strategies, where retrieval techniques exclusively depend on the depression of brightness temperatures by scattering by ice particles for radiometric measurements of rainfall over land. To examine this point, we further divide the scatter diagrams for TMI in Fig. 9 into oceanic and continental rainfalls. Figure 10 shows separate diagrams for each type of TMI-derived rainfall over ocean and land areas. The correlation between rain rate and precipitation water is excellent in an oceanic environment, whereas scatterplots are much more widely dispersed over land areas. The best-fit lines for Fig. 10 are

$$\mathrm{RR} = \begin{cases} -0.0032 + 20.3\mathrm{PWC}_{\mathrm{ns}} \\ \quad \text{for TMI (over ocean)} \quad \text{and} \\ -0.0020 + 19.5\mathrm{PWC}_{\mathrm{ns}} \\ \quad \text{for TMI (over land)} \end{cases} \tag{6}$$

for $\mathrm{PWC}_{\mathrm{ns}}$ and

$$\mathrm{RR} = \begin{cases} -0.0064 + 0.004\,21\mathrm{PWP} \\ \quad \text{for TMI (over ocean)} \quad \text{and} \\ -0.0019 + 0.004\,77\mathrm{PWP} \\ \quad \text{for TMI (over land)} \end{cases} \tag{7}$$

for PWP. Comparison of (6) and (7) with (3) and (4) reveals that the dependence on the surface condition (ocean or land) in TMI measurements is very small in comparison with the difference from PR measurements. Hence, the overall conclusions derived from Fig. 9 with (3) and (4) are unchanged for oceanic and continental rainfalls.

4. Summary and conclusions

In this paper, we compare TRMM standard rainfall products derived by the TMI (2A12) and PR (2A25) profiling algorithms to clarify the origins of the disagreement among the products pointed out by Kummerow et al. (2000). In our strategy, we focus on the precipitation water content and the precipitation water path, given by the vertical integration of PWC, for comparison instead of the rain rate that is usually of interest. This approach enables us to separate the intrinsic problems involved in the physical principles of remote sensing from the uncertainties resulting from the conversion from precipitation water to rain rate. We adopted two sets of monthly data (July of 1998 and January of 1999) for the analysis.

PWP and near-surface PWC, or $\mathrm{PWC}_{\mathrm{ns}}$, in the zonal mean generally show good agreement between the TMI and PR products except in midlatitude winter for PWC, where PR-$\mathrm{PWC}_{\mathrm{ns}}$ exceeds TMI-$\mathrm{PWC}_{\mathrm{ns}}$ (Fig. 1), and around the tropical rainfall maximum for PWP, where TMI-PWP exceeds PR-PWP (Fig. 2). These discrepancies are attributed to characteristic differences in the hydrometeor profiles retrieved by the TMI and PR algorithms, which are examined in terms of CFADs as a function of PWC (instead of the conventional definition of the radar reflectivity). Direct comparison between the PR- and TMI-derived PWC profiles is justified below the freezing level because of the insensitivity of PR to pure ice particles.

As a general trend, TMI shows very little variety in the PWC profiles in comparison with PR, which presents significant variations in the profiles corresponding to a wide range of precipitation characteristics from tropical convective rainfall to midlatitude storms. This invariability in the TMI-retrieved rainfall may be responsible for the underestimation of TMI-PWP in midlatitudes, implying a limitation of the preexisting database incorporated in the current TMI profiling algorithm. The PR measurements are liable to suffer from ambiguity in the attenuation correction in heavy precipitation around the tropical rainfall maximum, which is presumed to be the cause of the underestimation of near-surface PWC by PR in the Tropics.

It is meaningful to demonstrate how the discrepancies in PWC and PWP influence the rain rate in response to meteorological and hydrological interests. Scatter diagrams for $\mathrm{PWC}_{\mathrm{ns}}$ and PWP versus rain rate indicate that TMI tends to yield a larger rain rate than PR does for a given $\mathrm{PWC}_{\mathrm{ns}}$ or PWP, which is more significant for heavier precipitation. As a consequence, an excess of TMI in precipitation water over PR would be increased in terms of rain rate and vice versa. This bias accounts for the characteristics in the zonal mean monthly rain rate (Fig. 8), where the TMI products show a large excess in the tropical rain rate over the PR products but the discrepancy is reduced in the midlatitudes, consistent with Kummerow et al. (2000). Summarizing all the above findings, we conclude that the disagreement in the rainfall products between TMI and PR is a combined result of the intrinsic bias originating from the different physical principles between TMI and PR measurements and the purely algorithmic bias inherent in the conversion from precipitation water to rain rate.

This paper is a starting point toward development of an ultimate rainfall algorithm by combined use of a radar and a radiometer. There are unresolved issues such as the DSD uncertainty problem addressed in section 1. Furthermore, in contrast to this work, which is based on monthly averages, instantaneous matching of TMI and PR data would provide a greater insight into the origins of the disagreement in the retrievals. Although these topics are left to future studies, we have some implications from the current study that may be useful for future development of rainfall algorithms using either a microwave radiometer or a radar, or their combination.

As one may expect, difficulties in determining the vertical profiles from radiometric measurements and uncertainties in the attenuation correction for radar measurements are crucial obstacles to precise estimation of rainfall. The Bayesian approach based on a preexisting database as adopted in the TMI profiling algorithm (2A12) could be greatly improved by enriching the database to cover a wider variety in possible rainfall profiles. A combined algorithm using radiometric brightness temperatures at low frequencies to constrain the total attenuation in radar measurements (Haddad et al. 1997) would also be an efficient way to overcome the problems. More formidable problems are involved in ambiguities in the conversion from precipitation water to rain rate because a DSD and $v(D)$, required to evaluate (1), and their regional variations are uncertain. Nevertheless, the achievement of reasonable agreement in

rain rate requires significant reduction of the discrepancy in the conversion from precipitation water to rain rate among the algorithms.

A consistency study for rainfall products between radiometric and radar measurements will also be helpful in algorithm development for the TRMM follow-on project, currently being planned, in which a spaceborne dual-frequency precipitation radar with an additional channel at 35 GHz is being examined along with a successor of TMI. The addition of a higher-frequency radar channel would require a more precise correction of attenuation but would provide information about the DSD. This would eliminate many of the ambiguities that remain in PWP, PWC, and the surface rainfall. The Global Precipitation Measurement (GPM) mission is being planned in which a constellation of eight satellites carrying microwave radiometers is to be organized along with the TRMM follow-on satellite described above as a core satellite. It is required for GPM to develop a radiometer algorithm for the constellation satellites that takes advantage of the dual-frequency radar aboard the core satellite for improving accuracy of the retrieval. A possible solution is to update the current TMI (2A12) algorithm by incorporating radar-retrieved rainfall profiles in some way into the database. Efforts to sophisticate rainfall algorithms using spaceborne radar and radiometer are now being started with a view toward use in future projects in planning, such as GPM.

Acknowledgments. The authors greatly appreciate the assistance of S. Harada [Remote Sensing Technology Center of Japan (RESTEC)], who made a great effort to prepare and to reprocess the data products. They are also grateful to T. Kozu (Shimane University) and T. Higashiuwatoko (RESTEC) for preparing the lookup table for deriving the *Z–W* relations. They appreciate comments and suggestions provided by the anonymous reviewers, which were helpful for improving the paper. They thank H. Hanado (Communication Research Laboratory), S. Shige (NASDA/EORC), and T. Nomaki (RESTEC) for their discussions. TMI (2A12) and PR (2A25) data were provided by NASA GSFC.

REFERENCES

Aonashi, K., A. Shibata, and G. Liu, 1996: An over-ocean precipitation retrieval using SSM/I multichannel brightness temperatures. *J. Meteor. Soc. Japan,* **74,** 617–637.

Haddad, Z. S., E. A. Smith, C. D. Kummerow, T. Iguchi, M. R. Farrar, S. L. Durden, M. Alves, and W. S. Olson, 1997: The TRMM ''day-1'' radar/radiometer combined rain-profiling algorithm. *J. Meteor. Soc. Japan,* **75,** 799–809.

Iguchi, T., T. Kozu, R. Meneghini, J. Awaka, and K. Okamoto, 2000: Rain-profiling algorithm for the TRMM precipitation radar. *J. Appl. Meteor.,* **39,** 2038–2052.

Kidder, S. Q., and T. H. Vonder Haar, 1995: *Satellite Meteorology: An Introduction.* Academic Press, 466 pp.

Kummerow, C., and K. Giglio, 1994: A passive microwave technique for estimating rainfall and vertical structure information from space. Part I: Algorithm description. *J. Appl. Meteor.*, **33,** 3–18.

——, W. Olson, and K. Giglio, 1996: A simplified scheme for obtaining precipitation and vertical hydrometeor profiles from passive microwave sensors. *IEEE Trans. Geosci. Remote Sens.,* **34,** 1213–1232.

——, and Coauthors, 2000: The status of the Tropical Rainfall Measuring Mission (TRMM) after two years in orbit. *J. Appl. Meteor.*, **39,** 1965–1982.

Meneghini, R., T. Iguchi, T. Kozu, L. Liao, K. Okamoto, J. A. Jones, and J. Kwiatkowski, 2000: Use of the surface reference technique for path attenuation estimates from the TRMM precipitation radar. *J. Appl. Meteor.*, **39,** 2053–2070.

Olson, W., 1989: Physical retrieval or rainfall rates over the ocean by multispectral microwave radiometry: Application to tropical cyclones. *J. Geophys. Res.,* **94,** 2267–2280.

——, C. Kummerow, G. M. Heymsfield, and L. Giglio, 1996: A method for combined passive–active microwave retrievals of cloud and precipitation profiles. *J. Appl. Meteor.*, **35,** 1763–1789.

Spencer, R. W., 1986: A satellite passive 37-GHz scattering-based method for measuring oceanic rain rates. *J. Climate Appl. Meteor.*, **25,** 754–766.

Tao, W.-K., and Coauthors, 2001: Retrieved vertical profiles of latent heat release using TRMM rainfall products for February 1998. *J. Appl. Meteor.*, **40,** 957–982.

Viltard, N., C. Kummerow, W. S. Olson, and Y. Hong, 2000: Combined use of the radar and radiometer of TRMM to estimate the influence of drop size distribution on rain retrievals. *J. Appl. Meteor.,* **39,** 2103–2114.

Wilheit, T. T., A. T. C. Chang, M. S. V. Rao, E. B. Rodgers, and J. S. Theon, 1977: A satellite technique for quantitatively mapping rainfall rates over the oceans. *J. Appl. Meteor.,* **16,** 551–560.

——, ——, and L. S. Chiu, 1991: Retrieval of monthly rainfall indices from microwave radiometric measurements using probability distribution functions. *J. Atmos. Oceanic Technol.,* **8,** 118–136.